SSRG International Journal of Electrical and Electronics Engineering
ISSN: 2348-8379/ https://doi.org/10.14445/23488379/IJEEE-V11I3P115

Volume 11 Issue 3, 187-200, March 2024

Original Article

Grid Integrated Hybrid PV/Wind/FC System Using Bat Algorithm Based PI Controlled Luo Converter

Monika Singh[1], Siddheswar Kar[2], Murali Matcha[3], Nishant Dwivedi[4]

[1,2,3,4]*Department of Electrical Engineering, Medi-Caps University, Madhya Pradesh, India.*

[1]*Corresponding Author : singhmonika13071996@gmail.com*

Received: 10 January 2024 Revised: 07 February 2024 Accepted: 08 March 2024 Published: 25 March 2024

Abstract - *In recent years, Photovoltaic (PV), Wind Turbine (WT) and Fuel Cell (FC) Hybrid Renewable Energy Sources (HRES) have been used to reduce greenhouse gas emissions and energy consumption. PV and wind are the primary renewable energy sources, with fuel cells serving as supplemental sources to compensate for power fluctuations and ensure uninterrupted power delivery to the load. Grid-connected systems comprise renewable generation systems and distributed loads that operate under system control and grid-connected mode. However, the growing amount of clean energy sources and distributed generators necessitates novel approaches for the operation and management of the electricity grid for the purpose of increasing power-supply consistency. Thus, this work introduces a novel combined Luo converter along with a Bat optimization-based Proportional Integral (PI) controller for a hybrid PV/wind/FC system to enlarge and uphold the reliability of power supply to the grid system. Owing to the intermittent nature of the PV system, the output of the PV panel gets fluctuates, resulting in poor voltage and unable to meet the load demand. With the implementation of the Luo converter, the unregulated DC output is regulated with high efficiency and reduced current ripples. Furthermore, the Bat-optimized PI controller efficiently maintains the constant DC link voltage with improved dynamic response. The Boost converter is employed to strengthen the low output voltage of the fuel cell. Finally, the entire developed system is executed in MATLAB /Simulink in order to validate the proposed system's working functionality.*

Keywords - *Bat optimized PI controller, Boost converter, HRES, Luo converter, MATLAB / Simulink, PV / wind / FC system.*

1. Introduction

Energy is a key component of a sustainable economy and the engine of a country's social and economic development. Energy sources ought to be reliable, safe and environmentally benign [1, 2]. Human life requires energy usage, and modern society cannot survive without a reliable and plentiful supply. Government policy is promoting the use of RESs since the majority of energy comes from traditional sources that contribute to pollution. In addition, electricity is sometimes only available for a few hours in several locations [3, 4].

Several RESs are integrated into a Hybrid Energy System (HES), which offers a workable solution to meet the world's power demand and the electricity shortage at such locations [5]. The widespread use of RESs has been prompted by the development of smart grid capability, which fundamentally alters the conventional network architecture. To meet the peak load demand, a HES typically consists of two or more RESs [6, 7].

With benefits including high overall efficiency and low environmental impact, PV, wind, and Fuel Cell (FC) are the most popular RESs [8], which are utilized in this work. This offers a workable remedy for the energy problem, lowers CO_2 emissions and improves power grid dependability. However, power quality is still compromised, and the hybrid system obtains unstable and poor voltage, to improve the voltage, the DC-DC converter is necessitated [9, 10].

Various conventional converters are employed to boost the low voltage generated by the PV system. Conventional Buck and Buck-boost in [11, 12] is employed to improve the voltage from PV systems; such systems have an issue where high-frequency current harmonics are introduced in order to remove it, the system needs passive input filters, which adds bulk and expense to the system [13].

In contrast to buck-boost converters, the Cuk [14] and SEPIC [15] converters can provide voltage conversion ratios that are both higher and lower, and their input current is continuous. However, both of these converters have the drawback of having an important amount of input current ripples [16].

Therefore, the implemented work incorporated with the Luo converter for producing high efficiency reduces the ripple

content in voltage and current with reduced switching losses. Additionally, selecting an appropriate controller is crucial for enhancing the converter's dynamic performance, achieving unity power factor and lowering THD.

When used in a set range, the traditional PI [17] controller method is easy to use and efficient but inappropriate in non-linear operating situations. In the event of shocks and uncertainties, the PI controller responds slowly and experiences peak overshoot issues. [18] Optimization techniques have recently been used to control and enhance the behaviour of complex systems. However, evolutionary optimization is being used for good purposes by researchers quite rapidly and generally.

In [19] PSO, Artificial Bee Colony [20] and Whale Optimization Algorithm [21] are thought to have benefited greatly for their robustness, high flexibility and high computation efficiency. However, those optimization algorithms' primary drawbacks include their propensity for slow convergence, poor local optimization abilities, limited precision and inadequate population variety [22, 23].

To conquer the above mentioned limits, the proposed work utilized the Bat optimization algorithm, which characteristics include resilience, simplicity, less number of parameters and ease of implementation with rapid convergence speed. The following provides an illustration of the developed work's contribution.

- In order to continuously supply electricity to the grid, a separate voltage source converter is used to implement the grid-connected hybrid renewable system.
- By utilizing the Luo converter, the low voltage attained by the PV system gets efficiently boosted.
- The bat optimization algorithm-based PI controller is employed to provide rapid convergence speed with robustness.

2. Proposed Modelling

Various electrical power generation sources are referred to as hybrid energy systems. In this system, several renewable energy sources are combined, either independently or in conjunction with traditional energy sources, to make up for the erratic nature of RES and boost overall energy efficiency.

As a consequence, this work presents the grid-integrated hybrid PV/wind/FC system using bat algorithm based PI controlled Luo converter, and the block diagram for the implemented framework is represented in Figure 1, which is described as follows.

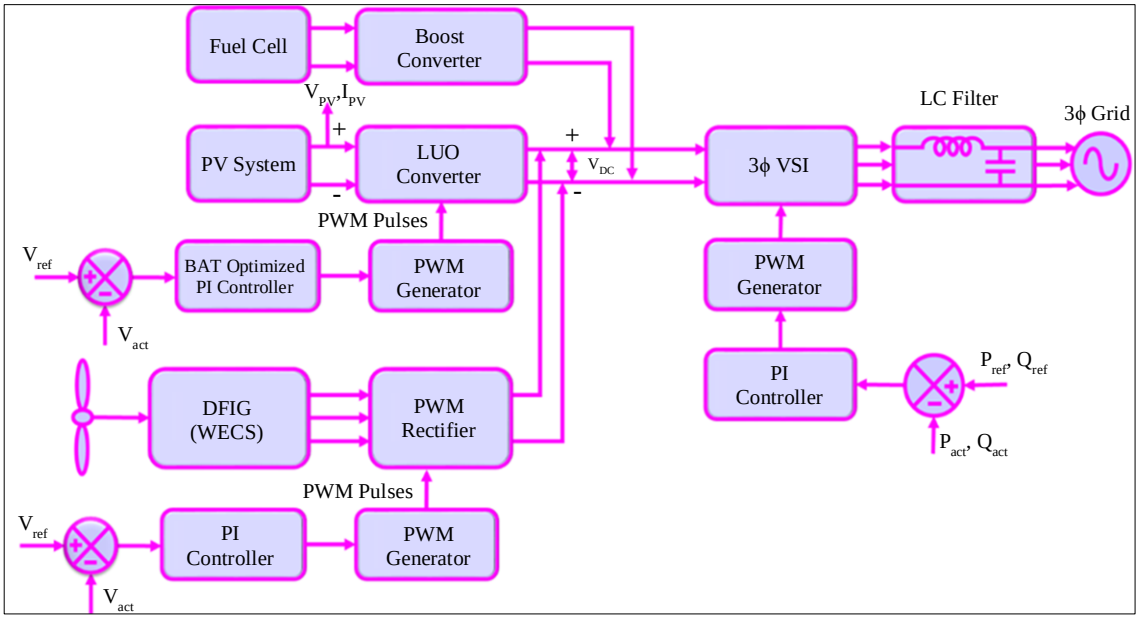

Fig. 1 Block diagram for the proposed framework

The PV system's output voltage is low due to its ecological changes, which are boosted by the developed Luo converter with high efficiency and reduced ripple current. The implemented converter is constantly stabilized by utilizing the Bat-optimized PI controller, and the controlled output is fed to the PWM generator to give pulses for better function of the Luo converter. On the other hand, the DFIG-based wind energy system provides the AC supply, which is converted into DC by adopting the PWM rectifier. V_{act} Actual voltage and reference voltage V_{ref} is compared, which generates the error signal.

PI controller and PWM pulses compensate for the error signal produced by the PWM generator for better functioning of the PWM rectifier. Moreover, the energy obtained from the fuel cell gets improved by employing the boost converter.

The enhanced and controlled DC link voltage is delivered to a three-phase VSI to convert the AC supply for delivery into the grid system, which is controlled by the PI controller. Finally, a constant and uninterrupted power supply is supplied to the grid system with the help of the proposed system.

2.1. Modelling of PV System

Solar PV panels convert solar radiation into DC electricity to ensure power generation. A solar cell module, also known as a photovoltaic module, is made up of frequent solar cells installed on a surface and connected in series or parallel to improve power production. The one-diode equivalent circuit is used to represent the PV cells, as shown in Figure 2. Equation 1 is utilized to ascertain the PV current.

$$I = I_{ph} - I_o\left[e^{(V+I_{Rs}} * \frac{q}{nkTN_S-1}\right] - \frac{(V+I_{Rs})}{R_{sh}} \qquad (1)$$

Where, T represents the absolute temperature, I_{ph} indicates the light produced current, n denotes the linearity factor, k specifies the Boltzmann gas constant, R_{sh} refers to the cell shunt resistance, V represents the output voltage of the solar cell, R_s indicates the cell series resistance and I_o indicates the dark saturation current value respectively.

The voltage obtained from the PV system is low due to its climatic variations, which is enhanced by implementing the Luo converter described below.

2.2. Modelling of Luo Converter

This study employs a Luo converter to boost the low voltage attained from the PV system. This converter has two inductors, one diode, one switch and two capacitors, as illustrated in Figure 3. Capacitors C_1,C_2 and inductors L_1, L_2 are the energy storage passive elements, and R is the load resistance. The circuit can be split into two modes to evaluate the Luo converter's operation. The following Figure 4 indicates the modes of operation for the proposed Luo converter.

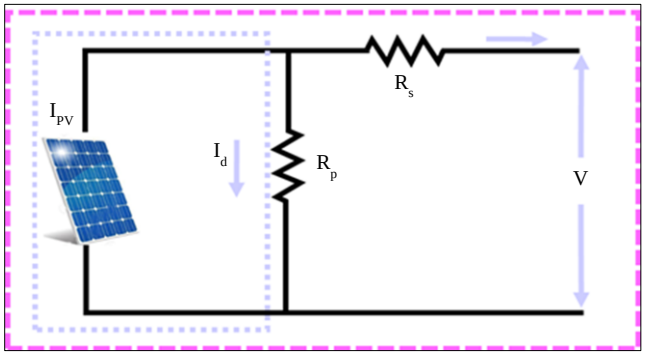

Fig. 2 Equivalent circuit diagram of PV system

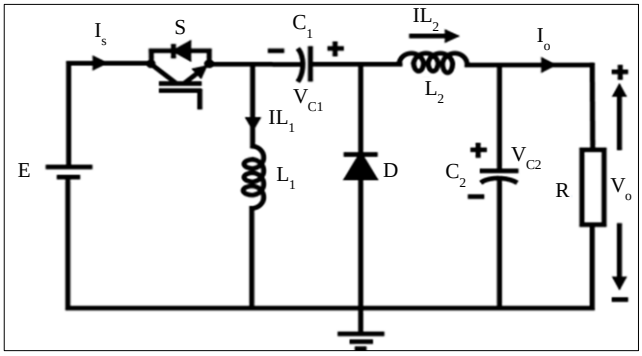

Fig. 3 Circuit diagram of Luo converter

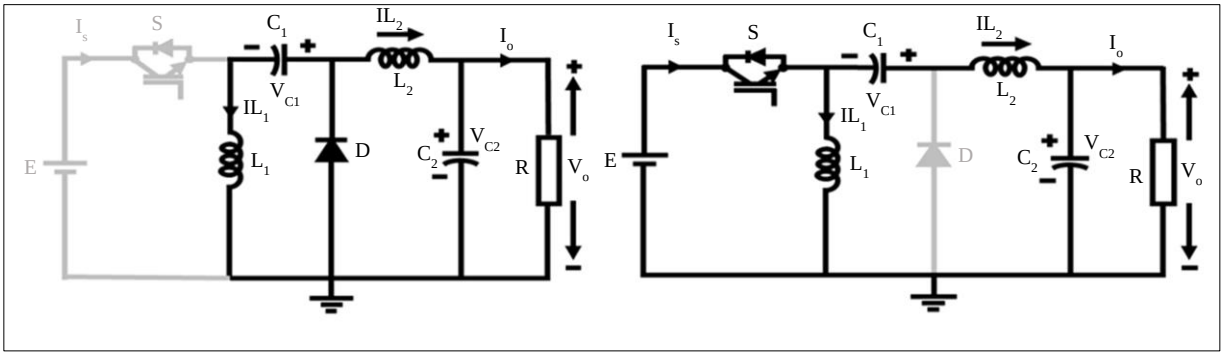

Fig. 4 Modes of operation (a) Mode 1, and (b) Mode 2.

Mode 1: The supply voltage charges the inductor L_1 during the switch is in the ON state. At the same time, the inductor L_2 absorbs the energy from the source as well as the capacitor C_1. The capacitor C_2 provides the load. The analogous circuit for a Luo converter operating in mode 1 is portrayed in Figure 4(a).

Mode 2: The current drawn from the source is zero when the switch is in the OFF position, as seen in Figure 4(b). The diode receives current iL_1 in order to charge the capacitor C_1. To maintain itself, the current iL_2 passes through the diode D and the C_2-R circuit.

2.2.1. Analysis of Luo Converter

The I_{L2} the inductor current is determined by the below equation,

$$I_{L2} = \frac{1-a}{a} I_{L1} \qquad (2)$$

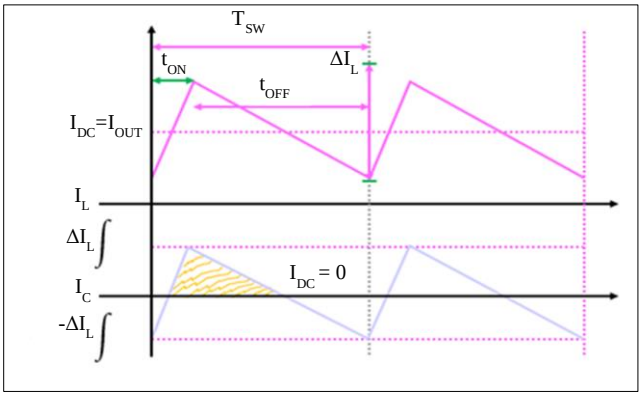

Fig. 5 Waveform for the proposed converter

The capacitor C_1 across the average voltage,

$$V_{c1} = \frac{a}{1-a} V_{in} \tag{3}$$

The inductor current peak-peak is determined as,

$$\nabla I_{l1} = \frac{\alpha T V_{in}}{L_1} \tag{4}$$

The inductor L_1 value as Equation 5 as,

$$L_1 = \frac{\alpha T V_{in}}{\nabla I_{L1}} \tag{5}$$

The inductor current L_2 peak to peak value is defined as,

$$\nabla I_{L2} = \frac{\alpha T V_{in}}{\nabla I_{L2}} \tag{6}$$

Following this, the proposed technique utilized a bat optimization algorithm to regulate the Luo converter, which is expressed as follows,

2.3. Modelling of Bat Algorithm

The bat algorithm is designed to resemble the way little bats use echolocation to find their way around in the dark, avoid obstacles, and spot openings.

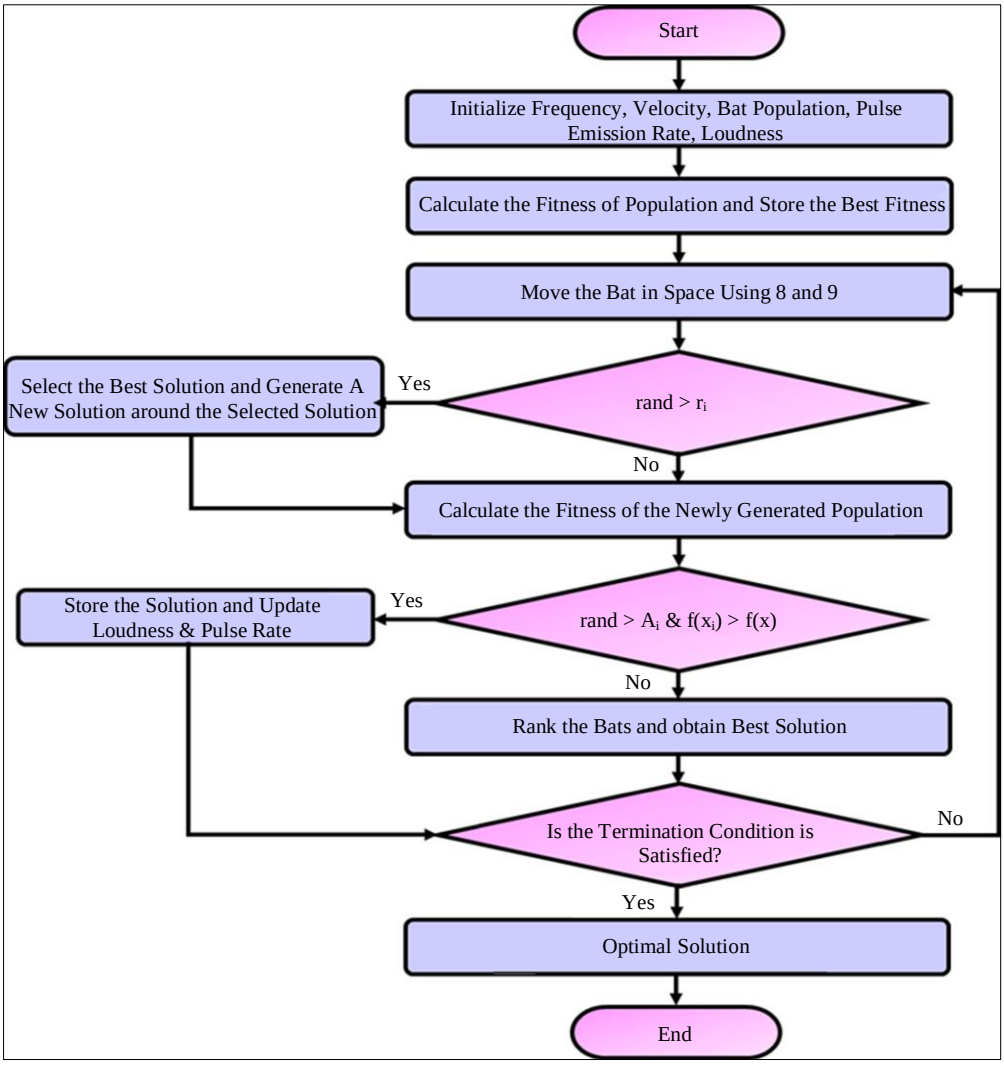

Fig. 6 Flowchart for the proposed Bat algorithm

Bats and certain other creatures use a navigational mechanism called echolocation, which uses sound signals to identify things in their surroundings. Every virtual bat in the original population updates its position inside the BA using a similar echolocation phenomena.

A sequence of powerful ultrasonic waves is delivered to produce echoes in the perceptual system bats use for echolocation. The bats analyze these waves, which return at varying audio levels and with delays, to identify a particular prey. The behaviour of bats employing the echolocation process can be summed up by the following laws, which form the basis of BA:

a) Every bat classifies its prey and obstacles based on the features of the echolocation process.
b) In order to reach their starting position x_i, bats fly at random at a speed v_i. They can also alter their frequency from f_{min} to f_{max}, as well as their wavelength (λ) and intensity (L) in order to find prey. The amount of pulses a bat emits varies on the proximity of its target or prey, and it can automatically modify the wavelength or frequency of the signal it emits.
c) From a constant lowest value L_{min} to a high-value L_0, the intensity or volume fluctuates. Every bat must have its xi position and v_i speed provided and updated in each BA iteration during the optimization process. The equations that follow provide guidelines for determining new bat solutions and velocities.

$$f_1 = f_{min} + (f_{max} - f_{min})rand \quad (7)$$

$$v_i^{i+1} = v_i^{t} + (x^* - x_i^{t})f_t \quad (8)$$

$$x_i^{t+1} = x_i^{t} + v_i^{i+1} \quad (9)$$

The intensity or volume varies from a fixed lowest value L_{min} to a high-value L_0. Throughout the optimization process, each bat's xi position and v_i speed must be supplied and updated for each BA iteration.

New bat solutions and velocities can be found using the following equations as a basis. From a fixed lowest value L_{min} to a high-value L_0, the intensity or volume fluctuates. Every bat must provide and update its xi position and v_i speed for every BA iteration during the optimization process.

Using the following equations as a guide, new bat solutions and velocities can be determined.

$$x_n = x_a + \epsilon^{L'} \quad (10)$$

Where x_a represents the best previous solution and x_n represents the new one. The average volume of all bats in iteration t is represented by L_t, while ε is a random value that falls between −1 and 1. The loudness can be changed to a useful value in the following manner: as the bats get closer to their meal, the intensity decreases and the number of pulses they produce increases.

$$L_i^{t+1} = \alpha + L_i^{t} \quad (11)$$

$$r_i^{t+1} = r_i^{0}(1 - e^{-\gamma t}) \quad (12)$$

Where γ is a constant value greater than zero, and α is a random constant between 0 and 1. The flowchart displayed in Figure 6 depicts the basic steps involved in the application of the BA algorithm. On the other hand, the DFIG-based wind energy system is implemented in this work, which is illustrated below.

2.4. DFIG Based Wind System Modelling

Windings from the stator and rotor make up the DFIG. It has rings made of slip, mounted on the stator and connected to the grid via a three-phase transformer or three-phase shielded windings. The rotor and stator are constructed using three-phase insulated windings. An external stationary circuit is connected to the rotor windings using a series of brushes and slip rings. Following Figure 7 indicates the equivalent circuit in the dq reference frame.

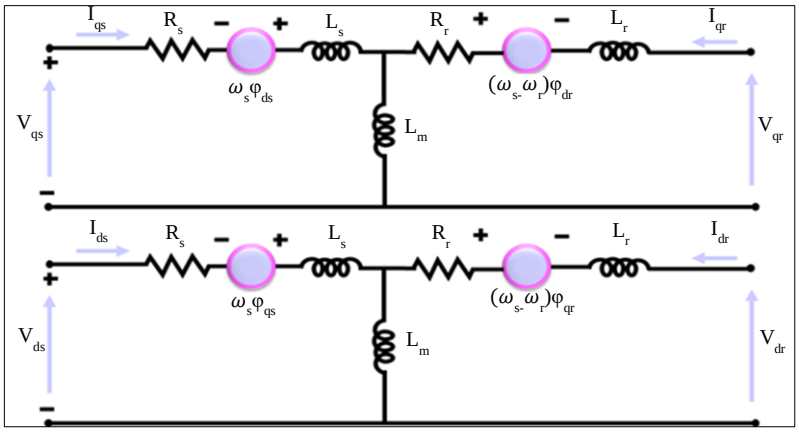

Fig. 7 Equivalent circuit in dq reference frame

The following equation provides a d–q reference frame for the dynamic modelling of a doubly-fed induction generator:

$$\begin{cases} V_{ds} = R_s I_{ds} + \frac{d}{dt}\varphi_{ds} - \omega_{ds} - \omega_s \varphi_{qs} \\ V_{qs} = R_s I_{qs} + \frac{d}{dt}\varphi_{qs} - \omega_s \varphi_{dr} \\ V_{dr} = R_r I_{dr} + \frac{d}{dt}\varphi_{dr} - (\omega_s - \omega_r)\varphi_{qr} \\ V_{qr} = R_r I_{qr} + \frac{d}{dt}\varphi_{dr} - (\omega_s - \omega_r)\varphi_{qr} \end{cases} \quad (13)$$

The rotor flux and stator are expressed as,

$$\begin{cases} \varphi_{ds} = L_s I_{ds} + L_m I_{dr} \\ \varphi_{qs} = L_s I_{qs} + L_m I_{qr} \\ \varphi_{dr} = L_s I_{dr} + L_m I_{ds} \\ \varphi_{qr} = L_r I_{qr} + L_m I_{qs} \end{cases} \quad (14)$$

The DFIG torque equation is given as follows

$$T_{em} = \frac{3}{2} p \frac{L_m}{L_r} \left(\varphi_{ds} I_{qr} - \varphi_{qs} I_{qr}\right) \quad (15)$$

The below Equation 16 indicates the stator's reactive and active powers,

$$\begin{cases} P_s = \frac{3}{2} V_{ds} I_{ds} + V_{qs} I_{qs} \\ Q_s = \frac{3}{2} V_{ds} I_{ds} - V_{qs} I_{qs} \end{cases} \quad (16)$$

The rotor's active power can be illustrated as

$$P_r = \frac{3}{2} (V_{dr} I_{dr} - V_{qr} I_{qr}) \quad (17)$$

Following this, another power generation source of fuel cell is utilized in this work that is described below.

2.5. Fuel Cell Modelling

A fuel cell is a device for converting chemical energy from hydrogen fuel into electrical energy by reacting positively charged hydrogen ions with oxygen to produce heat, water, and electricity. The following Equation 18 indicates the chemical reaction.

$$2H_2 + O_2 \rightarrow H_2O + electricity + heat \quad (18)$$

Equation 19 can be utilized to define the cell voltage as the difference between the total voltage losses in the fuel cell and the ideal Nernst voltage ENernst.

$$V_{FC} = E_{Nernst} - \sum \Delta V \quad (19)$$

The sum of voltage losses $\sum \Delta V$ is determined as below,

$$\sum \Delta V = V_{act} + V_{ohmic} + V_{con} \quad (20)$$

The thorough model of FC, which serves as a regulated voltage source, is displayed in Figure 8. This study uses a boost converter, explained below, to increase the fuel cell's voltage.

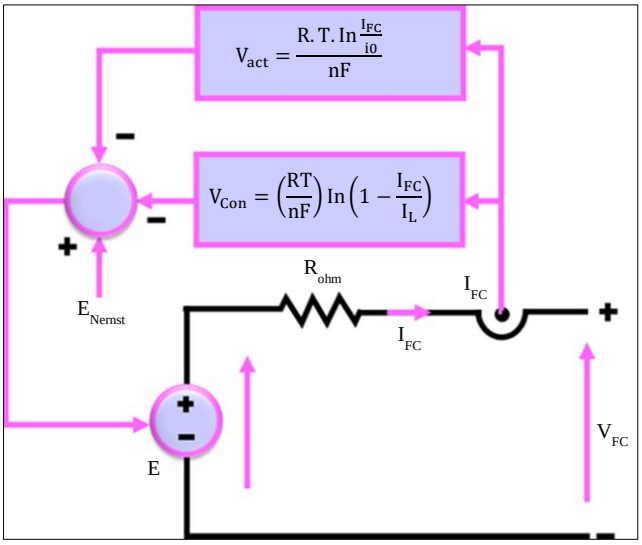

Fig. 8 Electrical model of fuel cell

2.6. Modelling of Boost Converter

The boost converter is utilized to raise input voltage to a greater level, and this converter has an inductor, a switch, a diode and a capacitor. Moreover, it has two modes of operation based on the switch's position. The inductor current increases when the switch is turned on because the output voltage is equal to the voltage across it. The current diminishes, and the inductor voltage equals (V_{in}−V_0).when the switch is turned OFF. Figures 9 and 10 display the circuit schematics of the Boost converter's equivalent circuits during switch ON and switch OFF conditions.

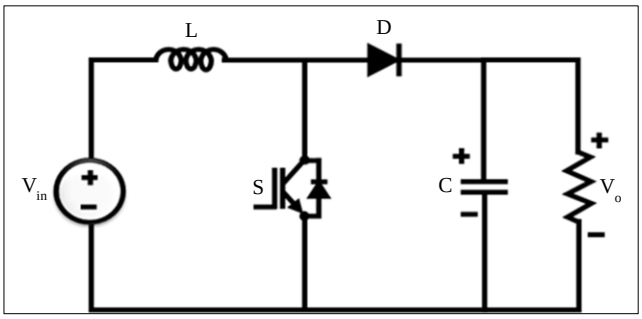

Fig. 9 Circuit diagram of boost converter

The duty cycle can be determined using the following formula:

$$k = 1 - \frac{V_{in}}{V_0} \quad (21)$$

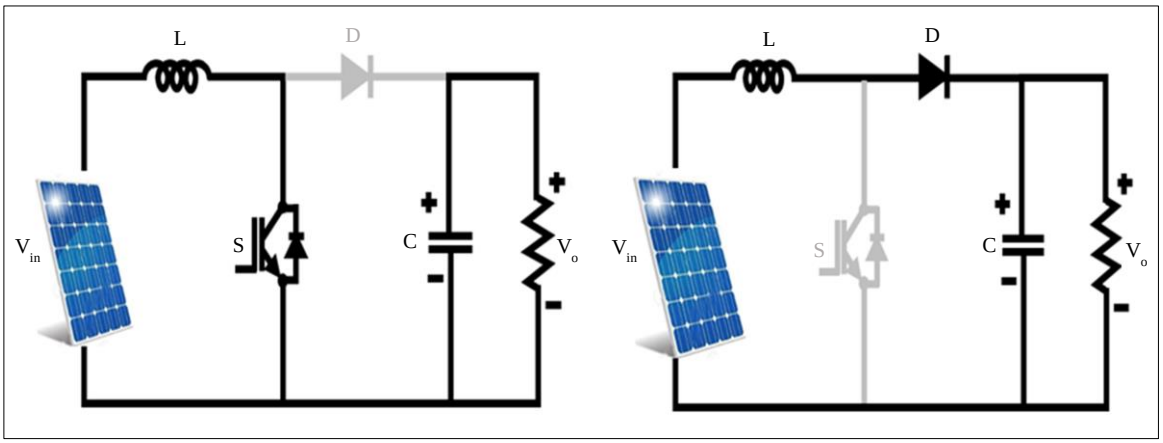

Fig. 10 Modes of operation (a) Mode 1, and (b) Mode 2.

Where voltages (V_{in} $-V_o$) for the input and output are located. As shown below, the load R_s is computed:

$$R_s = \frac{{V_0}^2}{P_{pv}} \tag{22}$$

Where P_{pv} represent the power of the solar panel. The following formulas are used to determine the input and output currents:

$$I_0 = \frac{V_0}{R_s} \tag{23}$$

$$I_{in} = \frac{I_0}{1-k} \tag{24}$$

The inductor value is estimated by,

$$L = \frac{kV_{in}}{f\Delta i_L} \tag{25}$$

Here, Δ denotes the ripple current and the capacitor value is defined as follows,

$$C = \frac{kV_0}{F\Delta v_c R_s} \tag{26}$$

Here, Δv_c specifies the ripple voltage.

3. Results and Discussion

The hybrid PV/wind/FC system using a bat algorithm-based PI-controlled Luo converter is implemented in this study. By exploiting the proposed converter and optimization topology, high efficiency, low THD, and less settling time with rapid convergence speed, The overall developed system is applied in MATLAB/Simulink to demonstrate the efficacy of the developed system.

The comparative analysis is represented as follows with various conventional topologies, and Table 1 specifies the parameter specification, which is defined below.

Table 1. Parameter specification

Parameter	Description
Solar PV System	
Open Circuit Voltage	12V
Peak Power	10kW, 10 panel
Series Connected Solar PV Cell	36
Short Circuit Current	8.3A
DFIG System	
Rotor Inductance	0.16mH (pu)
Pairs of Poles	3
No. of Turbines	4
Stator Resistance	0.023 Ω (pu)
Magnetizing Inductance	2.9mH
Rotor Resistance	0.016Ω (pu)
Line-Line Voltage	415V
Stator Inductance	0.18mH (pu)
Frequency	50Hz
Friction Factor	0.01F (pu)
Nominal Power	10kW

3.1. Case 1: Under Varying Condition

Figure 11 represents the solar panel waveform for the proposed system in case 1; from Figure 11(a), the temperature varied slightly up to 0.3s, and after 0.3s, the temperature was constantly upheld at 35C. Likewise, the irradiation of solar panels is constantly maintained at 1000 (W/Sq.m) after 0.3s,

as demonstrated in Figure 11(b). The voltage waveform is specified in Figure 11(c), which analyzed that after 0.3s the voltage gets continuously upheld at 80V after a certain oscillation. Also, as indicated in Figure 11(d), the current oscillated initially and after 0.4s, a constant current is upheld at 18A respectively. The converter output waveform for case 1 is illustrated in Figure 12, which states that the converter voltage using the PI controller highly raised initially and fluctuated after 0.4s; the constant voltage is preserved at 500V, as shown in Figure 12(a). Also, by utilizing the proposed Bat-PI controller, the voltage is highly oscillated for a certain period of time. After 0.1s, the voltage gets preserved at 600V, as indicated in Figure 12(b). Furthermore, the current waveform is given in Figure 12(c), which analyzed that the current slightly varied initially after 0.1s constant current is upheld at 3A.

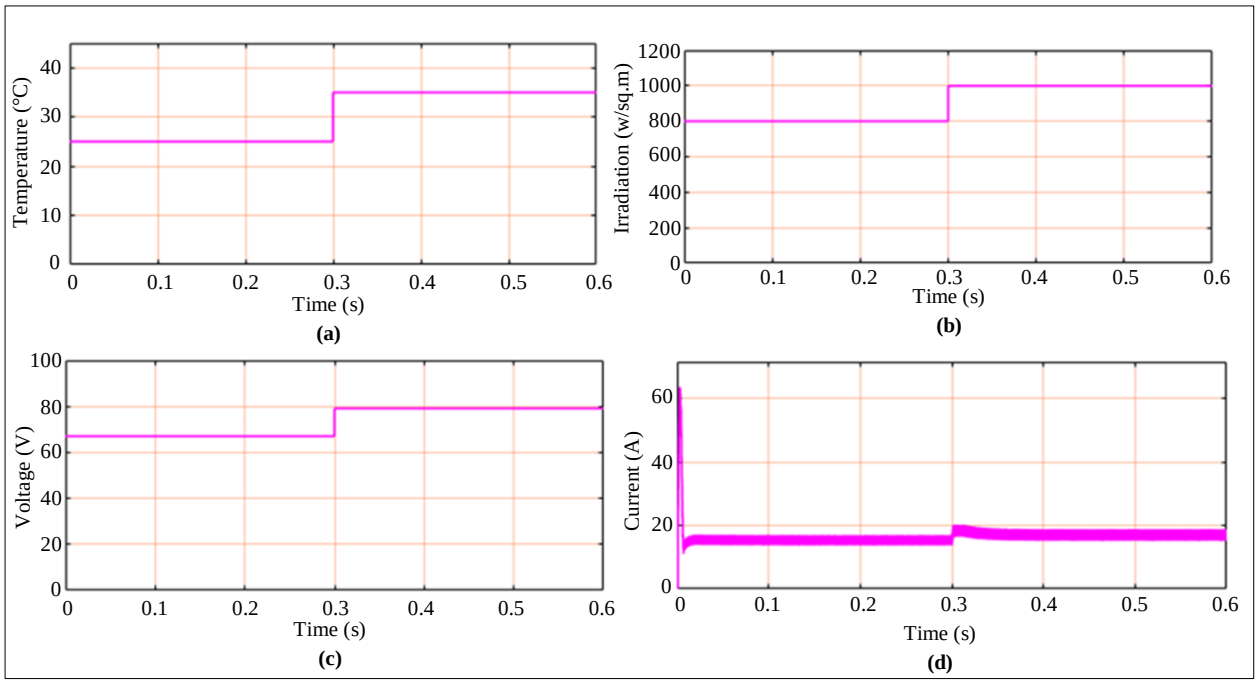

Fig. 11 Solar panel waveform for case 1 (a) Temperature, (b) Irradiation, (c) Voltage, and (d) Current.

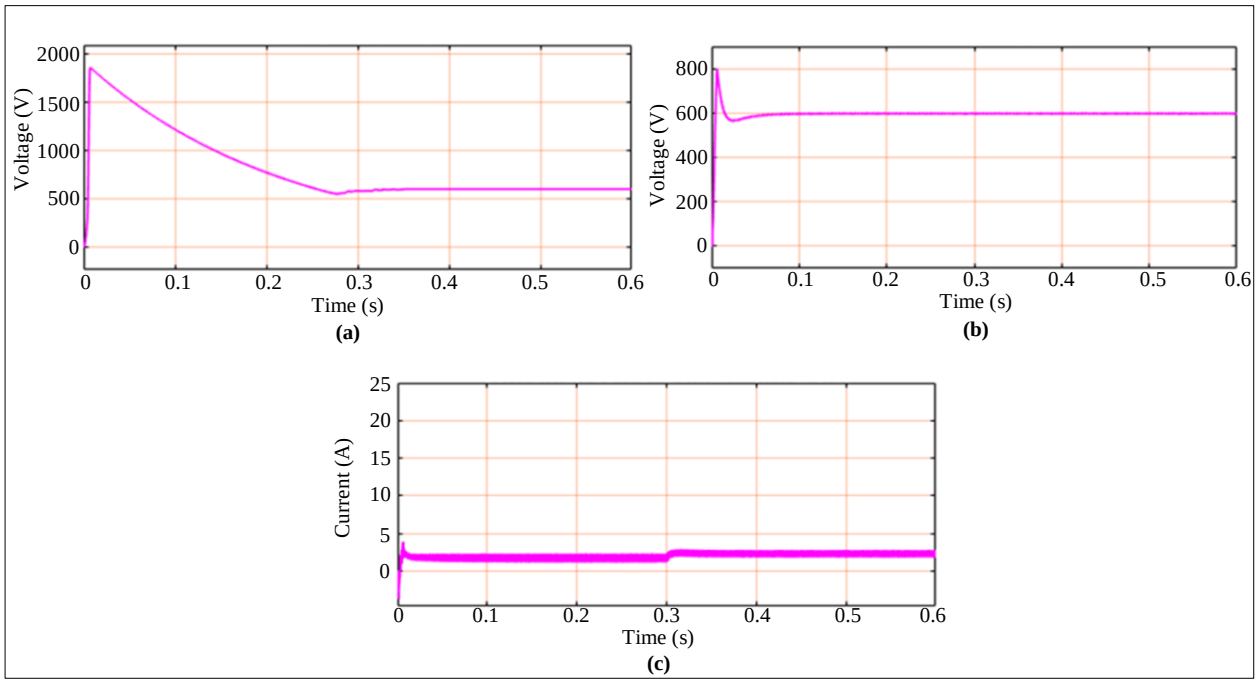

Fig. 12 Converter output waveform for case 1 (a) Voltage waveform using PI controller, (b) Voltage using Bat-PI controller, and (c) Current.

3.2. Case 2: At Constant Condition

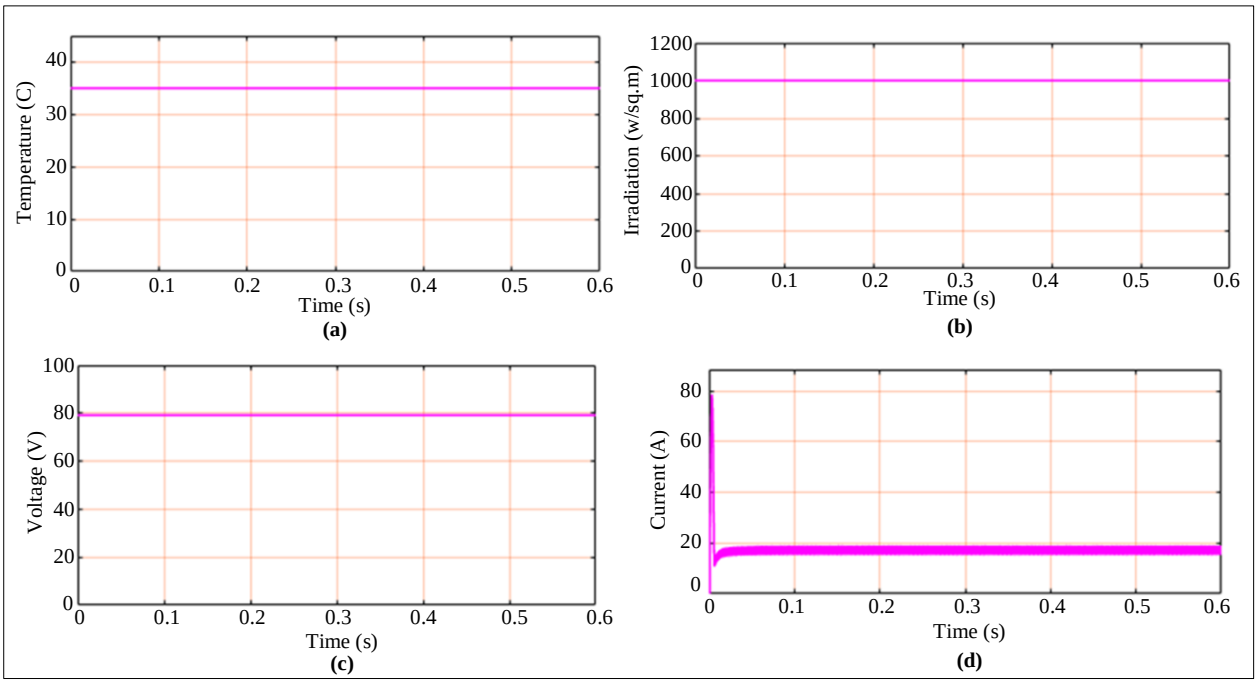

Fig. 13 Solar panel waveform for case 2 (a) Temperature, (b) Irradiation, (c) Voltage, and (d) Current.

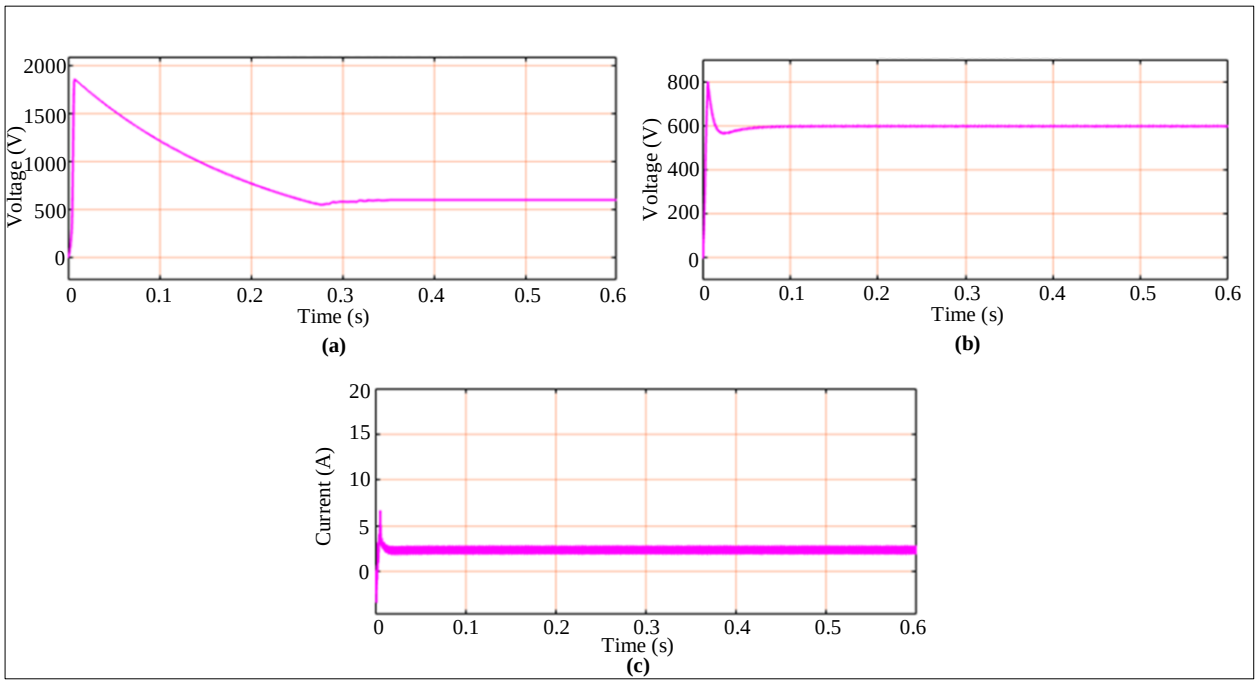

Fig. 14 Converter output waveform for case 2 (a) Voltage waveform using PI controller, (b) Voltage using Bat-PI controller, and (c) Current.

In Figure 13 for case 2, the solar panel waveform represented that the solar panel temperature and irradiation are constantly maintained at 35C and 1000(W/Sq.m) as specified in Figure 13(a). Likewise, the solar panel voltage and current are maintained constant at 80V, and the current is initially raised with fluctuation after 0.05s; it is constantly maintained at 18A, respectively, as indicated in Figure 13(d).

Figure 14 illustrates the converter output waveform; from the results, it is observed that the voltage varied highly at the initial time, and after 0.4s, the constant voltage is upheld at 500V by using the PI controller as specified in Figure 14(a). Similarly, Figure 14(b) represents the converter voltage using the proposed bat algorithm, which attained its constant voltage at 600V. Moreover, the converter output current oscillated at

the initial period, and after 0.08s it constantly upheld at 5A as indicated in Figure 14(c) correspondingly. The implemented fuel cell voltage is represented in Figure 15(a), and the current fluctuates at a certain period of time and after 0.3s, the constant voltage is upheld at 12A, respectively, as specified in Figure 15 (b).

Boost converter waveform is indicated in Figure 16 for case 2; as stated in Figure 16(a), the converter voltage is initially highly raised at a certain period of time. After 0.2s, the constant voltage is maintained upheld at 600V, and as represented in Figure 16(b), the current is highly oscillated and constantly maintained at 4A after 0.4s, respectively.

Figure 17 represents the DFIG and PWM rectifier waveform, from the result stated that the constant DFIG voltage gets constantly preserved at 600V, as represented in Figure 17(a). Additionally, the PWM rectifier output voltage is highly varied initially, and after 0.2s, the constant voltage is upheld at 600V, as specified in Figure 17(b).

The grid waveform for case 2 is illustrated in Figure 18; from Figure 18(a), the grid voltage is constantly maintained at 400V, and the grid current is upheld constantly at 12A, as specified in Figure 18(b). Also, the grid current and voltage are constantly maintained at 0A and 400V, respectively.

The power factor waveform is specified in Figure 19, and it is observed that the power factor gets continually upheld at 1(PU) after certain oscillations, as illustrated in Figure 19(a). Real and reactive power is accomplished at unity by utilizing the proposed system, as demonstrated in Figure 19 (b) and (c).

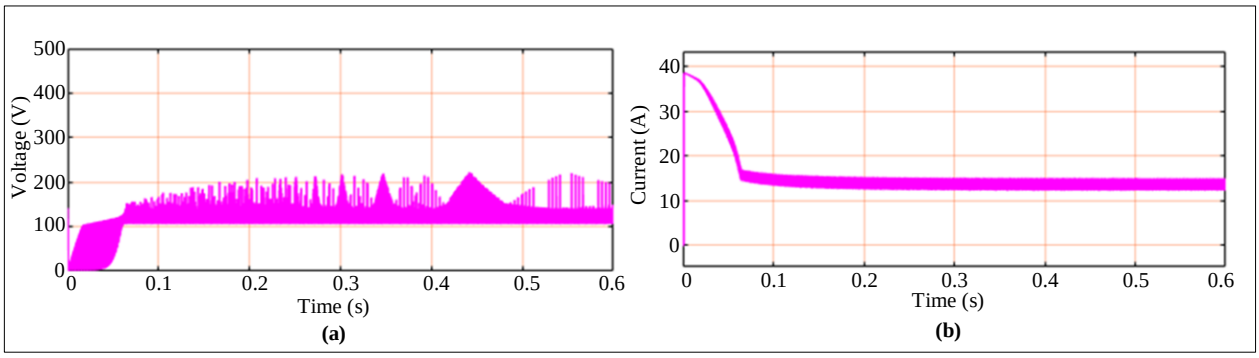

Fig. 15 Waveform for fuel cell (a) Voltage, and (b) Current.

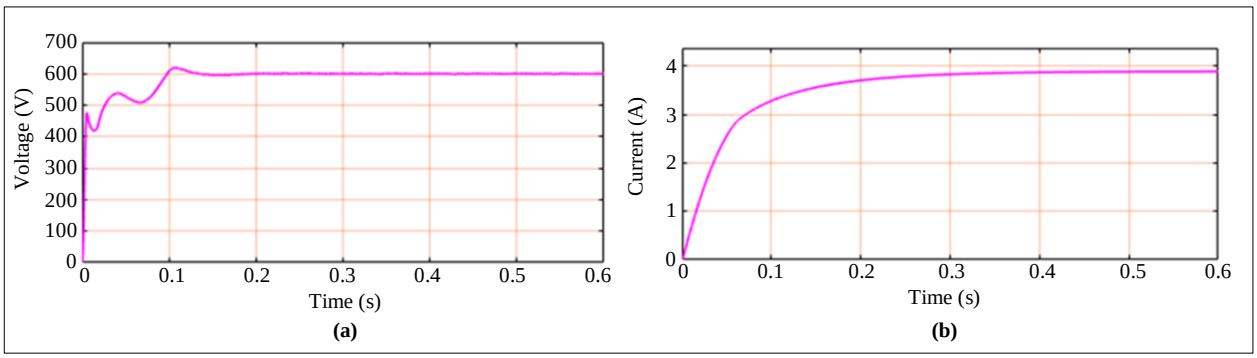

Fig. 16 Waveform for Boost converter (a) Voltage, and (b) Current.

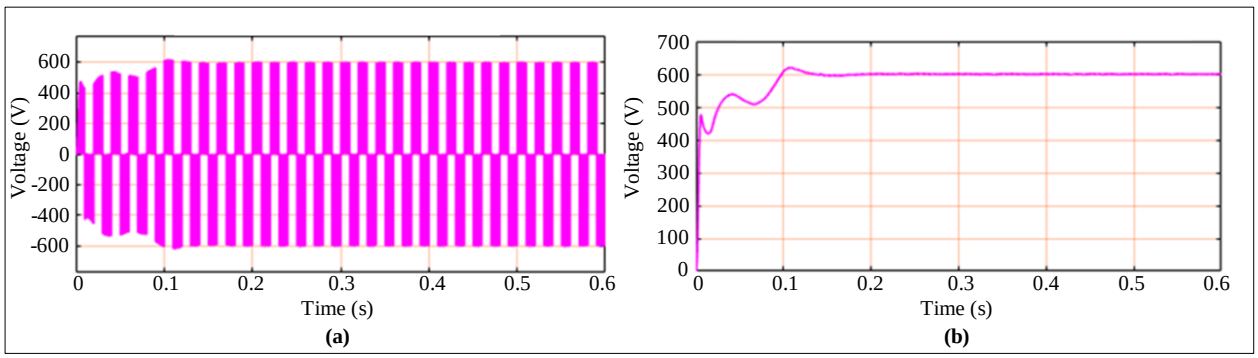

Fig. 17 Output voltage waveform (a) DFIG, and (b) PWM rectifier.

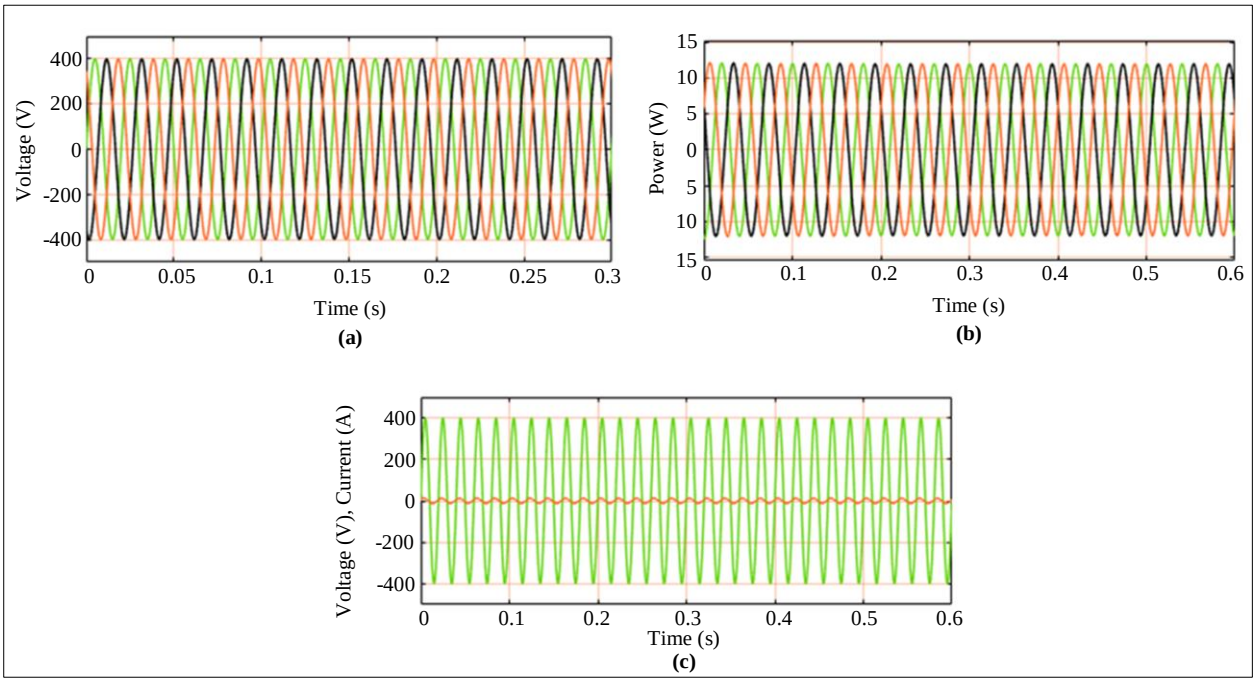

Fig. 18 Grid waveform (a) Voltage, (b) Current, and (c) Voltage and current,

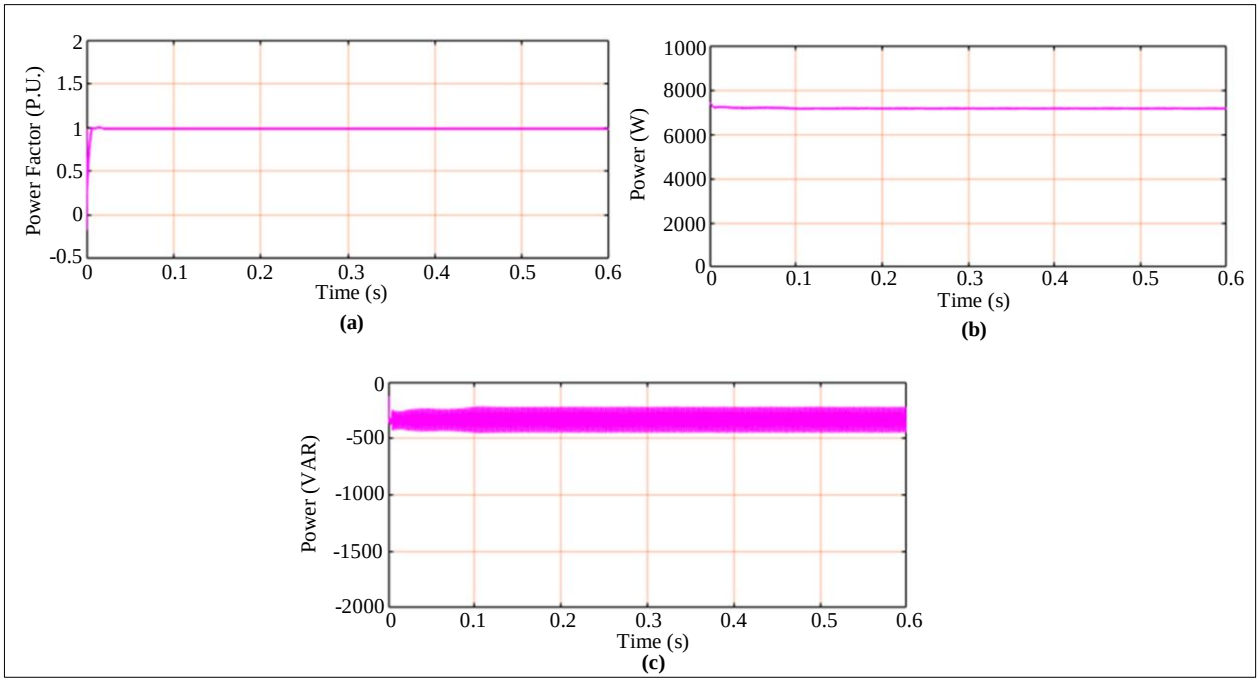

Fig. 19 Waveform for (a) Power factor, (b) Real power, and (b) Reactive power.

Table 2. Comparison of converter efficiency

Converters	Efficiency (%)
Boost [24]	80
Buck-Boost [25]	84
Cuk [14]	88
SEPIC [26]	80
Proposed converter	93.89

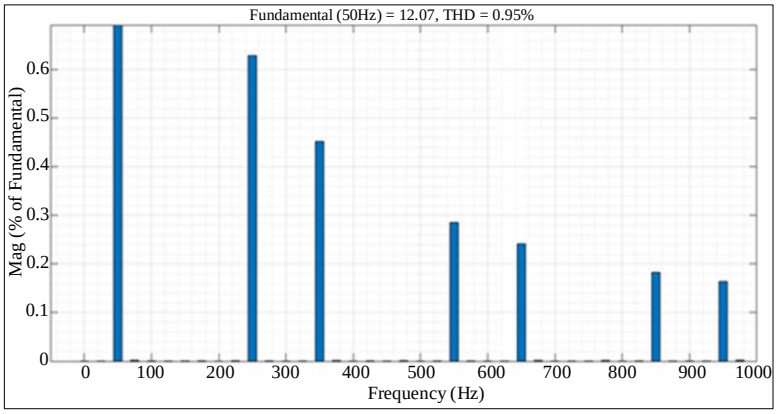

Fig. 20 THD waveform

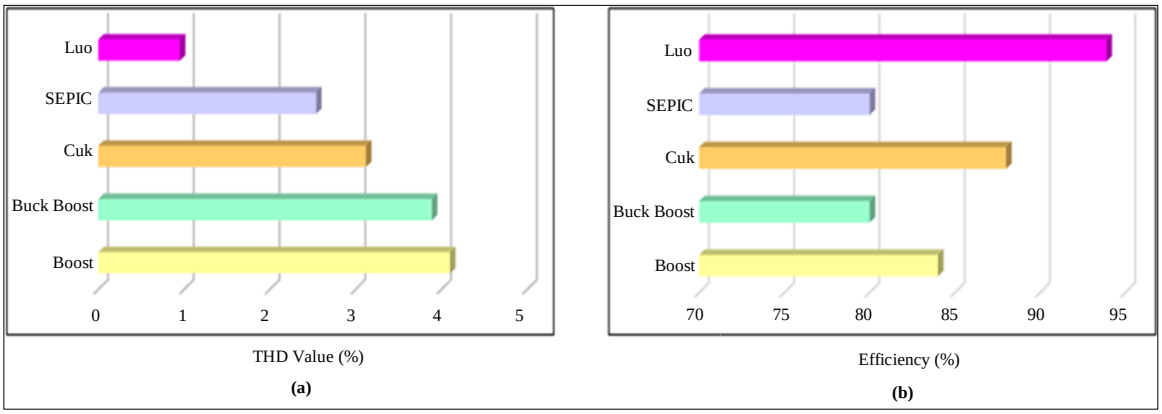

Fig. 21 Comparison of converter (a) THD value, and (b) Efficiency.

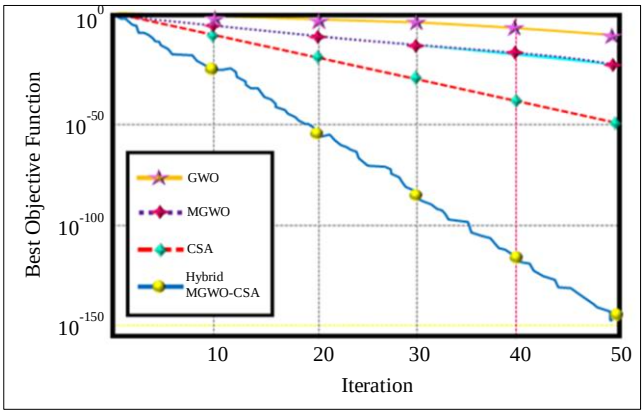

Fig. 22 Comparison of convergence speed

Table 3. Comparison of optimized controller

Controllers	Settling Time (s)	Rise Time (s)
PSO Optimized PID [27]	9.7825	0.5783
ABC Optimized PID [28]	5.57	0.261
FFA-PID [29]	0.32	0.23
Proposed	0.09	0.01

The proposed Luo converter THD value waveform is specified in Figure 20, which is analyzed that the developed converter attains 0.95% respectively. The proposed Luo converter achieved a high efficiency of 93.89% compared to the other conventional converters like Boost and Buck-boost, as evidenced by the comparison graph for converter THD value and efficiency in Figures 21(a), and 21(b).

Cuk and SEPIC are specified in Figure 21(a) and Table 2. Likewise, the THD value is obtained lower by utilizing the implemented converter with a value of 0.95% than the conventional converter topologies, as indicated in Figure 21(b).

Table 3 represents the optimized controller comparison, which analyzed that the proposed bat-PI controller achieves less settling time of 0.09s and rise time of 0.01s than the other conventional optimized topologies like PSO-PID, ABC-PID and FFA-PI algorithm.

The proposed Bat optimization algorithm is compared with the existing techniques like PSO, ABC and FFA, as specified in Figure 22, which states that the proposed algorithm achieves rapid convergence speed compared to the other topologies.

4. Conclusion

In this investigation, a hybrid PV/DFIG-based wind system and Fuel cell with Luo converter and Bat optimization algorithm are proposed to enlarge and preserve the reliability of power supply to the grid system. Owing to the ecological changes of the PV system, the output of the PV panel fluctuates, which is effectively boosted by the Luo converter with high efficiency, reduced switching losses and THD value. On the other hand, utilizing the Boost converter greatly enhances the voltage from the fuel cell. Furthermore, the proposed Luo converter is efficiently regulated by implementing the Bat-optimized PI controller, which has the ability to provide rapid convergence speed within less settling time. The overall established work is performed in MATLAB/Simulink, and the proposed topology is contrasted with the conventional techniques to show the proficiency of the developed work. As a result, the outcomes obtained from the comparison graph illustrate that the developed Luo converter has a high efficiency of 93.89% and a low THD value of 0.95%, and rapid convergence speed is achieved by the bat-optimized PI controller with less settling time of 0.09s than the existing topologies respectively.

References

[1] Armenia Androniceanu, and Oana Matilda Sabie, "Overview of Green Energy as A Real Strategic Option for Sustainable Development," *Energies*, vol. 15, no. 22, pp. 1-35, 2022. [CrossRef] [Google Scholar] [Publisher Link]

[2] Bing Li, "Effective Energy Utilization through Economic Development for Sustainable Management in Smart Cities," *Energy Reports*, vol. 8, pp. 4975-4987, 2022. [CrossRef] [Google Scholar] [Publisher Link]

[3] Zulfiqar Ali Baloch et al., "A Multi-Perspective Assessment Approach of Renewable Energy Production: Policy Perspective Analysis," *Environment, Development and Sustainability*, vol. 24, pp. 2164-2192, 2021. [CrossRef] [Google Scholar] [Publisher Link]

[4] Ambarish Panda et al., "Recent Advances in the Integration of Renewable Energy Sources and Storage Facilities with Hybrid Power Systems," *Cleaner Engineering and Technology*, vol. 12, 2023. [CrossRef] [Google Scholar] [Publisher Link]

[5] Jamiu O. Oladigbolu, Makbul A.M. Ramli, and Yusuf A. Al-Turki, "Feasibility Study and Comparative Analysis of Hybrid Renewable Power System for Off-Grid Rural Electrification in a Typical Remote Village Located in Nigeria," *IEEE Access*, vol. 8, pp. 171643-171663, 2020. [CrossRef] [Google Scholar] [Publisher Link]

[6] Francesco Pilati et al., "Intelligent Management of Hybrid Energy Systems for Techno-Economic Performances Maximisation," *Energy Conversion and Management*, vol. 224, 2020. [CrossRef] [Google Scholar] [Publisher Link]

[7] M.A. Hannan et al., "Optimized Controller for Renewable Energy Sources Integration into Microgrid: Functions, Constraints and Suggestions," *Journal of Cleaner Production*, vol. 256, 2020. [CrossRef] [Google Scholar] [Publisher Link]

[8] Mudathir Funsho Akorede, "Design and Performance Analysis of Off-Grid Hybrid Renewable Energy Systems," *Hybrid Technologies for Power Generation*, pp. 35-68, 2022. [CrossRef] [Google Scholar] [Publisher Link]

[9] Nikolaos Sifakis, Stefanos Konidakis, and Theocharis Tsoutsos, "Hybrid Renewable Energy System Optimum Design and Smart Dispatch for Nearly Zero Energy Ports," *Journal of Cleaner Production*, vol. 310, 2021. [CrossRef] [Google Scholar] [Publisher Link]

[10] Jianquan Liao et al., "Voltage Stability Improvement of a Bipolar DC System Connected with Constant Power Loads," *Electric Power Systems Research*, vol. 201, 2021. [CrossRef] [Google Scholar] [Publisher Link]

[11] Humam Al-Baidhani et al., "Simplified Nonlinear Voltage-Mode Control of PWM DC-DC Buck Converter," *IEEE Transactions on Energy Conversion*, vol. 36, no. 1, pp. 431-440, 2021. [CrossRef] [Google Scholar] [Publisher Link]

[12] Binxin Zhu et al., "Low-Voltage Stress Buck-Boost Converter with a High-Voltage Conversion Gain," *IEEE Access*, vol. 8, pp. 95188-95196, 2020. [CrossRef] [Google Scholar] [Publisher Link]

[13] Molla Shahadat Hossain Lipu et al., "Battery Management, Key Technologies, Methods, Issues, and Future Trends of Electric Vehicles: A Pathway toward Achieving Sustainable Development Goals," *Batteries*, vol. 8, no. 9, pp. 1-60, 2022. [CrossRef] [Google Scholar] [Publisher Link]

[14] Khaled A. Mahafzah et al., "A New Cuk-Based DC-DC Converter with Improved Efficiency and Lower Rated Voltage of Coupling Capacitor," *Sustainability*, vol. 15, no. 11, pp. 1-17, 2023. [CrossRef] [Google Scholar] [Publisher Link]

[15] Omar Abdel-Rahim et al., "Enhancing Photovoltaic Conversion Efficiency with Model Predictive Control-Based Sensor-Reduced Maximum Power Point Tracking in Modified SEPIC Converters," *IEEE Access*, vol. 11, pp. 100769-100780, 2023. [CrossRef] [Google Scholar] [Publisher Link]

[16] Neeraj Priyadarshi et al., "New CUK-SEPIC Converter Based Photovoltaic Power System with Hybrid GSA-PSO Algorithm Employing MPPT for Water Pumping Applications," *IET Power Electronics*, vol. 13, no. 13, pp. 2824-2830, 2020. [CrossRef] [Google Scholar] [Publisher Link]

[17] Carlos Aguilar-Ibanez et al., "PI-Type Controllers and Σ–Δ Modulation for Saturated DC-DC Buck Power Converters," *IEEE Access*, vol. 9, pp. 20346-20357, 2021. [CrossRef] [Google Scholar] [Publisher Link]

[18] Gurcan Cetin, Osman Ozkaraca, and Ali Kecebas, "Development of PID Based Control Strategy in Maximum Exergy Efficiency of a Geothermal Power Plant," *Renewable and Sustainable Energy Reviews*, vol. 137, 2021. [CrossRef] [Google Scholar] [Publisher Link]

[19] Md. Shafiul Alam, Fahad Saleh Al-Ismail, and Mohammad Ali Abido, "PV/Wind-Integrated Low-Inertia System Frequency Control: PSO-Optimized Fractional-Order PI-Based SMES Approach," *Sustainability*, vol. 13, no. 14, pp. 1-21, 2021. [CrossRef] [Google Scholar] [Publisher Link]

[20] Neelamsetti Kiran Kumar et al., "Fuzzy Logic-Based Load Frequency Control in an Island Hybrid Power System Model Using Artificial Bee Colony Optimization," *Energies*, vol. 15, no. 6, pp. 1-20, 2022. [CrossRef] [Google Scholar] [Publisher Link]

[21] K. Ranjitha et al., "Firefly Algorithm Optimized Load Frequency Controller for Multi-Source Power System," *Emerging Trends in Industry 4.0 (ETI 4.0)*, Raigarh, India, pp. 1-6, 2021. [CrossRef] [Google Scholar] [Publisher Link]

[22] Fazli Wahid et al., "An Enhanced Firefly Algorithm Using Pattern Search for Solving Optimization Problems," *IEEE Access*, vol. 8, pp. 148264-148288, 2020. [CrossRef] [Google Scholar] [Publisher Link]

[23] Xinyu Liu, Guangquan Li, and Peng Shao, "A Multi-Mechanism Seagull Optimization Algorithm Incorporating Generalized Opposition-Based Nonlinear Boundary Processing," *Mathematics*, vol. 10, no. 18, pp. 1-19, 2022. [CrossRef] [Google Scholar] [Publisher Link]

[24] Nabil Abouchabana et al., "Power Efficiency Improvement of a Boost Converter Using a Coupled Inductor with a Fuzzy Logic Controller: Application to a Photovoltaic System," *Applied Sciences*, vol. 11, no. 3, pp. 1-19, 2021. [CrossRef] [Google Scholar] [Publisher Link]

[25] R. Abhishek, Pallavi Zoting, and Purva Ragit, "Design and Analysis of a DC-DC Buck Converter and Boost Converter to Achieve High Efficiency by Altering Duty Cycle and Input Voltage," *International Journal of Scientific and Research Publications*, vol. 10, no. 6, pp. 731-738, 2020. [CrossRef] [Google Scholar] [Publisher Link]

[26] Jingying Hu et al., "High-Frequency Resonant SEPIC Converter with Wide Input and Output Voltage Ranges," *IEEE Transactions on Power Electronics*, vol. 27, no. 1, pp. 189-200, 2012. [CrossRef] [Google Scholar] [Publisher Link]

[27] Anju K. Vincent, and Ruban Nersisson, "Particle Swarm Optimization Based PID Controller Tuning for Level Control of Two Tank System," *IOP Conference Series: Materials Science and Engineering*, vol. 263, pp. 1-7, 2017. [CrossRef] [Google Scholar] [Publisher Link]

[28] Ahmed M. Mosaad, Mahmoud A. Attia, and Almoataz Y. Abdelaziz, "Whale Optimization Algorithm to Tune PID and PIDA Controllers on AVR system," *Ain Shams Engineering Journal*, vol. 10, no. 4, pp. 755-767, 2019. [CrossRef] [Google Scholar] [Publisher Link]

[29] Leandro Dos Santos Coelho, and Viviana Cocco Mariani, "Firefly Algorithm Approach Based on Chaotic Tinkerbell Map Applied to Multivariable PID Controller Tuning," *Computers & Mathematics with Applications*, vol. 64, no. 8, pp. 2371-2382, 2012. [CrossRef] [Google Scholar] [Publisher Link]